Photolithographic Polymerization of Diacetylene-Containing Phospholipid Bilayers Studied by Multimode Atomic Force Microscopy

ARTICLE *in* LANGMUIR · AUGUST 2003

Impact Factor: 4.46 · DOI: 10.1021/la034078f · Source: OAI

Photolithographic Polymerization of Diacetylene-Containing Phospholipid Bilayers Studied by Multimode Atomic Force Microscopy

Kenichi Morigaki,*[,†,§,||] Holger Schönherr,*[,†,‡,⊥] Curtis W. Frank,[†,‡] and Wolfgang Knoll[†,‡,§]

NSF MRSEC Center on Polymer Interfaces and Macromolecular Assemblies (CPIMA), Department of Chemical Engineering, Stanford University, Stanford, California 94305-5025, and Max-Planck-Institute for Polymer Research, 55128 Mainz, Germany

Received January 16, 2003. In Final Form: January 28, 2003

Photopolymerization of the diacetylene-containing phospholipid 1,2-bis(10,12-tricosadiynoyl)-*sn*-glycero-3-phosphocholine (**1**) in substrate-supported planar lipid bilayers (SPBs) has been studied by using multimode atomic force microscopy (AFM). Monolayers and bilayers of **1** have been transferred onto glass substrates by the Langmuir−Blodgett (LB) and Langmuir−Schaefer (LS) techniques, respectively. Bilayers of monomeric **1** were removed easily from the substrate surface by detergent solutions (0.08 M sodium dodecyl sulfate (SDS)). Once they were photopolymerized by UV light, the bilayers became resistant toward detergent solubilization or exposure to air. High-resolution AFM images revealed the molecular packing of the hydrocarbon tails and the headgroups for monolayers and bilayers, respectively. The lattice spacing of photopolymerized **1** bilayers was similar to that of monomeric bilayers, suggesting that the polymerization proceeds without disruption of the bilayer structure. Patterned SPBs of poly-**1** were obtained by UV photolithography and selective removal of the protected monomeric bilayers. AFM revealed that the photopolymerization proceeds heterogeneously within the bilayers, depending on the UV irradiation dose. At longer UV exposure times, side reactions and/or reorganization of the molecules within the bilayer may occur.

Introduction

The modification of solid surfaces with biological molecules is currently studied with the aim of developing biomimetic interfaces that will play key roles in numerous biomedical and environmental applications. Among various proposed formats of functionalized interfaces, substrate-supported planar lipid bilayers (abbreviated as SPBs in the following) provide a unique possibility for reconstituting cellular membranes on a solid surface.[1,2] SPB micropatterning has attracted considerable attention because it allows the creation of designed microarrays of biological materials and should facilitate various new applications, such as high throughput drug screening.[3−7]

We have recently reported a novel SPB micropatterning strategy based on the lithographic photopolymerization of the diacetylene phospholipid 1,2-bis(10,12-tricosadiynoyl)-*sn*-glycero-3-phosphocholine (**1**).[8,9] The fabrication process comprises four steps (a schematic illustration is given in Figure 1): (i) formation of a monomeric bilayer on a solid substrate, (ii) lithographic photopolymerization by UV light, (iii) removal of the unpolymerized bilayers, and (iv) refilling the empty areas with new lipid bilayers. The lipid bilayers, which are incorporated at the last step, retain some characteristic features of native cellular membranes (e.g., lateral fluidity) and are intended to be used for further biological applications. Since the defined matrix of the polymerized lipid bilayer templates is prepared in the first three steps, these steps are essential for the current micropatterning strategy.

We have employed diacetylene phospholipid **1** for the photopolymerization of lipid bilayers (Figure 2). Photopolymerization of this and similar diacetylenes proceeds in the solid state (topochemical polymerization) and results in rigid films.[10−12] Preorganization of the diacetylene moieties can be achieved in Langmuir−Blodgett (LB) films and self-assembled monolayers (SAMs). These assemblies based on diacetylene-containing amphiphiles have been investigated as potential photoresist materials.[13−16]

* Corresponding authors.
† CPIMA.
‡ Stanford University.
§ Max-Planck-Institute for Polymer Research.
|| Present address: National Institute of Advanced Industrial Science and Technology (AIST), Ikeda 563-8577, Japan. Fax: +81-72-751-9628. E-mail: morigaki-kenichi@aist.go.jp.
⊥ Present address: University of Twente, Faculty of Science and Technology and MESA+ Research Institute, Department of Material Science and Technology of Polymers, P.O. Box 217, 7500 AE Enschede, The Netherlands. Fax: +31-53-489-3823. E-mail: h.schonherr@ct.utwente.nl.

(1) Sackmann, E. *Science (Washington, D.C.)* **1996**, *271*, 43−48.
(2) Plant, A. *Langmuir* **1993**, *9*, 2764−2767.
(3) Groves, J. T.; Ulman, N.; Boxer, S. G. *Science (Washington, D.C.)* **1997**, *275*, 651−653.
(4) Jenkins, A. T. A.; Boden, N.; Bushby, R. J.; Evans, S. D.; Knowles, P. F.; Miles, R. E.; Ogier, S. D.; Schönherr, H.; Vancso, G. J. *J. Am. Chem. Soc.* **1999**, *121*, 5274−5280.
(5) Cremer, P. S.; Yang, T. *J. Am. Chem. Soc.* **1999**, *121*, 8130−8131.
(6) Groves, J. T.; Mahal, L. K.; Bertozzi, C. R. *Langmuir* **2001**, *17*, 5129−5133.
(7) Fang, Y.; Frutos, A. G.; Lahiri, J. *J. Am. Chem. Soc.* **2002**, *124*, 2394−2395.
(8) Morigaki, K.; Baumgart, T.; Offenhäusser, A.; Knoll, W. *Angew. Chem., Int. Ed. Engl.* **2001**, *40*, 172−174.
(9) Morigaki, K.; Baumgart, T.; Jonas, U.; Offenhäusser, A.; Knoll, W. *Langmuir* **2002**, *18*, 4082−4089.
(10) Wegner, G. *Makromol. Chem.* **1972**, *154*, 35−48.
(11) *Polydiacetylenes*; Cantow, H.-J., Ed.; Springer-Verlag: Berlin, 1984.
(12) *Polydiacetylenes: Synthesis, Structure and Electronic Properties*; Bloor, D., Chance, R. R., Eds.; Martinus Nijhoff Publishers: Dordrecht/Boston/Lancaster, 1985.
(13) Barraud, A. *Thin Solid Films* **1983**, *99*, 317−321.
(14) Batchelder, D. N.; Evans, S. D.; Freeman, T. L.; Häussling, L.; Ringsdorf, H.; Wolf, H. *J. Am. Chem. Soc.* **1994**, *116*, 1050−1053.
(15) Chan, K. C.; Kim, T.; Schoer, J. K.; Crooks, R. M. *J. Am. Chem. Soc.* **1995**, *117*, 5875−5876.

10.1021/la034078f CCC: $25.00
Published on Web 07/19/2003

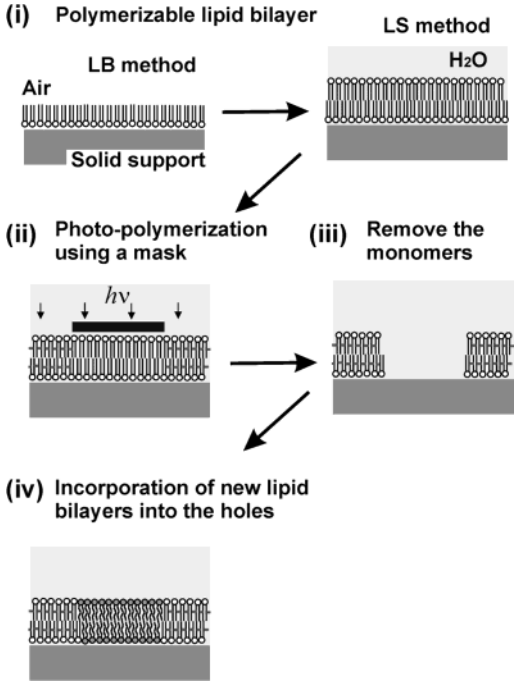

Figure 1. Schematic of the strategy employed for the micropatterning of lipid bilayer membranes.

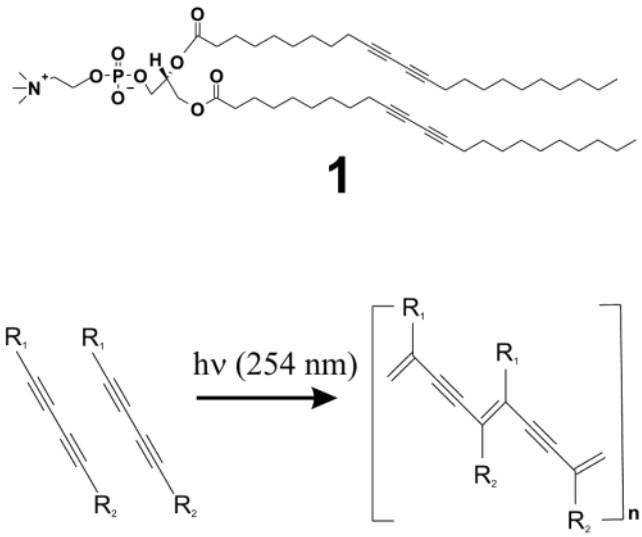

Figure 2. Polymerizable diacetylene phospholipid **1** and the polymerization scheme.

Poly(diacetylenes) form long conjugated sequences of ene−yne backbones, which absorb UV/visible light strongly. This property has attracted much attention because of potential optical and electronic applications. In particular, the reversible and nonreversible color changes due to the structural transition between blue and red polymorphs of poly(diacetylenes) have been studied extensively for colorimetric sensor applications.[17−21] Furthermore, diacetylene-containing phospholipids have been polymerized in lipid vesicles (liposomes) with the aim of producing mechanically robust drug carrier capsules.[22−26] It has been also reported that some chiral diacetylene phospholipids form unique tubular structures in water if they are incubated below the solid−fluid phase transition temperature (T_c) of the bilayers.[27,28] Various applications of these tubules have also been proposed.[29]

In previous work, we have obtained information on the successful photopatterning strategy mainly relying on the specific fluorescence of the polymer backbones.[8,9] Herein we report on the complementary real-space characterization of the morphology and nanometer-scale order of the layers by multimode atomic force microscopy (AFM) during all steps of the fabrication process. Although polymerized monolayers of diacetylene-containing adsorbates have been studied extensively by scanning probe methods,[30−33] this is the first report of an AFM investigation of the nanometer-scale structure and morphology of unpolymerized and polymerized bilayers of diacetylene phospholipids. Our observations shed light on the underlying processes of our micropatterning strategy and may lead to the development of various technical improvements.

Materials and Methods

Materials. Diacetylene phospholipid (**1**), 1,2-bis(10,12-tricosadiynoyl)-*sn*-glycero-3- phosphocholine, was purchased from Avanti Polar Lipids (Alabaster, AL); sodium dodecyl sulfate (SDS) was purchased from Fluka (Buchs, Switzerland); all other chemicals were purchased from Sigma (St. Louis, MO). These commercially obtained chemicals were used without further purification. As substrates for the SPBs, we have used either microscopy glass slides (Menzel, Braunschweig, Germany), polished quartz (Hellma, Müllheim, Germany), or silicon wafers.

Substrate Cleaning. The substrates were cleaned first with a commercial detergent solution (0.5% Hellmanex/water, Hellma, Mühlheim, Germany), rinsed with deionized water, treated in a warm solution of 28% NH_4OH/30% H_2O_2/H_2O (1:1:5) (65 °C for 15 min), rinsed extensively with deionized water, and then dried in a vacuum oven at 110 °C. This protocol resulted in clean and hydrophilic surfaces for the adsorption of lipid bilayer membranes.

Preparation of Supported Planar Bilayers. Monolayers and bilayers of monomeric **1** were deposited onto solid substrates from the air/water interface using a KSV5000 Langmuir trough (KSV Instruments, Helsinki, Finland). Diacetylene lipid **1** was spread from a chloroform solution. The lipids formed stable monolayers at the air/water interface up to a surface pressure of 40 mN/m at 20 °C. The monolayers were transferred onto solid substrates at 35 mN/m (fully condensed state). The first monolayer was deposited by dipping and withdrawing the substrate vertically (Langmuir−Blodgett (LB) method). The second leaflet was deposited onto the hydrophobic surface of the

(16) Mowery, M. D.; Smith, A. C.; Evans, C. E. *Langmuir* **2000**, *16*, 5998−6003.
(17) Charych, D. H.; Nagy, J. O.; Spevak, W.; Bednarski, M. D. *Science (Washington, D.C.)* **1993**, *261*, 585−588.
(18) Okada, S.; Peng, S.; Spevak, W.; Charych, D. *Acc. Chem. Res.* **1998**, *31*, 229−239.
(19) Jonas, U.; Shah, K.; Norvez, S.; Charych, D. H. *J. Am. Chem. Soc.* **1999**, *121*, 4580−4588.
(20) McQuade, D. T.; Pullen, A. E.; Swager, T. M. *Chem. Rev.* **2000**, *100*, 2537−2574.
(21) Kolusheva, S.; Boyer, L.; Jelinek, R. *Nature Biotechnol.* **2000**, *18*, 225−227.
(22) Hub, H.-H.; Hupfer, B.; Koch, H.; Ringsdorf, H. *Angew. Chem., Int. Ed. Engl.* **1980**, *19*, 938−940.
(23) Johnston, D. S.; McLean, L. R.; Whittam, M. A.; Clark, A. D.; Chapman, D. *Biochemistry* **1983**, *22*, 3194−3202.
(24) Ringsdorf, H.; Schlarb, B.; Venzmer, J. *Angew. Chem., Int. Ed. Engl.* **1988**, *27*, 113−158.
(25) Freeman, F. J.; Chapman, D. In *Liposomes as Drug Carriers*; Gregoriadis, G., Ed.; John Wiley & Sons: New York, 1988; pp 821−839.
(26) Mueller, A.; O'Brien, D. F. *Chem. Rev.* **2002**, *102*, 727−757.
(27) Yager, P.; Schoen, P. E. *Mol. Cryst. Liq. Cryst.* **1984**, *106*, 371−381.
(28) Schnur, J. M.; Ratna, B. R.; Selinger, J. V.; Singh, A.; Jyothi, G.; Easwaran, K. R. K. *Science (Washington, D.C.)* **1994**, *264*, 945−947.
(29) Schnur, J. M. *Science (Washington, D.C.)* **1993**, *262*, 1669−1676.
(30) Marti, O.; Ribi, H. O.; Drake, B.; Albrecht, T. R.; Quate, C. F.; Hansma, P. K. *Science (Washington, D.C.)* **1988**, *239*, 50−52.
(31) Nelles, G.; Schönherr, H.; Jaschke, M.; Wolf, H.; Schaub, M.; Küther, J.; Tremel, W.; Bamberg, E.; Ringsdorf, H.; Butt, H. J. *Langmuir* **1998**, *14*, 808−815.
(32) Sasaki, D. Y.; Carpick, R. W.; Burns, A. R. *J. Colloid Interface Sci.* **2000**, *229*, 490−496.
(33) Okawa, Y.; Aono, M. *Nature (London)* **2001**, *409*, 683−684.

first monolayer by pressing the substrate horizontally through the monolayer at the air/water interface and dropping it into the subphase (Langmuir−Schaefer (LS) method). The deposition of the second monolayer was typically made 1−2 h after the first. After the deposition of the second monolayer, the samples were collected from the trough and stored in deionized water (in the dark).

Photopolymerization of Bilayers. The polymerization was conducted in a closed system that comprised a water reservoir, a pump, and a cell (ca. 4 mL volume) equipped with a quartz window using a small low pressure mercury lamp (2 W, strong emission band at 254 nm, UVP, Pen-Ray, Upland, CA) as the light source. Prior to polymerization, argon-purged oxygen-free water was circulated continuously by the pump (3.8 mL/min) through the polymerization cell for typically 15 min.[34] UV photopatterning was achieved by illuminating the SPB through a contact mask (gold pattern on quartz), which was mounted onto the sample inside the cell. The distance between the UV light source and the SPB was 5 cm.

Solubilization of Layers of Lipid 1 by Detergent. Non-polymerized **1** molecules were removed from the substrate surface with SDS solutions. The film thickness of monolayers and bilayers of **1** was measured by ellipsometry in air (L116C, Gaertner, Chicago, IL, wavelength 632.8 nm, 70° angle of incidence, polarizer set to 45°) after treatment in various concentrations of SDS. Silicon wafers were used as substrates for these experiments. Since the ellipsometry measurements were conducted in air, the measured thickness of the bilayers was an average value of the collapsed films. By contrast, the thicknesses of monolayers were measured for *intact* films.

Atomic Force Microscopy. The AFM experiments were carried out on a NanoScope III (Digital Instruments (DI), Santa Barbara, CA) in contact mode (CM) and tapping mode (TM). For CM-AFM V-shaped Si_3N_4 cantilevers with various spring constants were used (regular tips, Nanoprobes (DI), $k_{nominal} = 0.06-0.58$ N/m; oxide sharpened tips, Olympus, $k_{nominal} = 0.02$ N/m). The triangular Si_3N_4 cantilevers with $k_{nominal} = 0.58$ N/m were also used for TM-AFM in water. The TM-AFM data in air were acquired with single beam Si cantilevers (Nanosensors, Wetzlar, Germany, $\nu_0 \approx 300$ kHz). Measurements were performed as specified in air (30%−40% humidity, 24 °C ambient temperature)[35] or liquid (Milli-Q water or solutions of SDS in Milli-Q water, temperature inside the liquid cell ca. 30−32 °C) using a DI liquid cell. The scanner was protected against liquid spillage by covering the top part with a very thin film of sealant (Parafilm, American National Can, Neenah, WI). For most experiments under liquid, the rubber ring was *not* used since the samples were glued to the sample holder using pressure-sensitive adhesive and since the maximum scan range without distortions due to rubber ring flexing is not compromised. The use of pressure-sensitive adhesive was necessary to mount samples onto the AFM while keeping the surface, which was later imaged, covered by water at all times. For this purpose, the rubber ring was pressed under water onto the sample supported on a glass slide. The slide and the rubber ring were taken out of solution and placed onto a sheet of adsorbent paper to dry the bottom side of the slide. If necessary, water was refilled into the rubber ring using a syringe. Next, the sample was transferred onto the sample holder, which was covered with double-sided, pressure-sensitive adhesive. The holder was mounted onto the protected scanner with minimal delay. Then the rubber ring was removed and additional water was deposited onto the sample, ensuring that the water spanned the distance between the sample and the liquid cell of the AFM after the AFM head was put onto the scanner. After a brief equilibration period of typically several minutes necessary to obtain a stable photodiode reading, the experiments were started. For high-resolution CM-AFM measurements under water, the samples were glued with epoxy (Devcon 5 Minute Epoxy, ITW Devcon, Danvers, MA) to the sample holder disk. Here the AFM liquid cell was used *with* the rubber ring. Equilibration times of up to 6 h ensured that thermal and instrumental drift were minimized. CM-AFM experiments in liquid and in air were carried out with controlled forces adjusted according to the additionally recorded force−distance plots. Usually the lowest possible imaging force was used (<200 pN). The operating conditions in tapping mode in liquid and in air were also adjusted to minimal peak forces by keeping the undamped amplitude as low as possible and maintaining a high set-point amplitude ratio. All the images shown here were subjected to a first-order plane-fitting procedure to compensate for sample tilt and, if necessary, to a zero-order flattening.

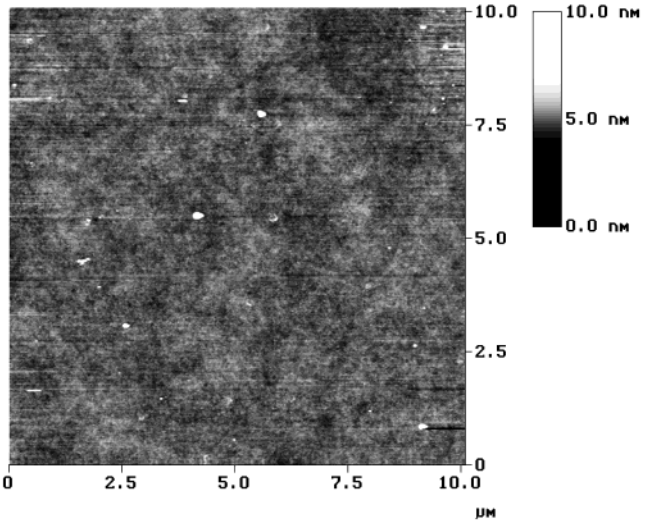

Figure 3. TM-AFM height image of a monolayer of monomeric **1** on glass acquired in air.

Results

The characterization of the monomeric monolayers and bilayers is described first. Following the discussion on the solubilization procedures, the photopolymerization of bilayers and the characterization of the obtained polymer layers will be described.

Morphology and Molecular Order in Monomeric Monolayers/Bilayers on Glass Substrates. Figure 3 shows a TM-AFM image of a monolayer acquired in air. Although scattered dust particles can be recognized, there are essentially no discernible defects present in the layer. Monolayers of monomeric **1** were very flat; the measured root-mean-square (rms) roughness was 0.3 ± 0.06 nm (scan size 5 μm × 5 μm), which is comparable to the glass substrates used in this study (0.4 ± 0.04 nm). At defect sites or intentionally induced scratches of the monomeric monolayer film, we measured an apparent layer thickness of ca. 1.3 nm. This step height does *not* correspond directly to the monolayer height since it is unlikely that the bare substrate is exposed at the defects observed (vide infra).

High-resolution images recorded in contact mode in air show a near-hexagonal periodic lattice structure with $d = 5.8$ Å (corresponding to an area per molecule of ca. 29 Å^2) (Figure 4a). These values compare favorably to the spacing/area requirement of individual hydrocarbon tails.

Prolonged storage of the monomer films in air led to reorganization of the film structure to a needlelike morphology. These needles showed a markedly different lattice structure at the surface as revealed by CM-AFM in air (Figure 4b). The restructured crystals form a lattice, which can be described as rectangular ($a_1 = 4.9$ Å, $b_1 = 7.3$ Å). The area requirement of 36 Å^2 per molecule suggests a significantly different orientation of the molecules compared to the as-transferred Langmuir monolayer (hexagonal lattice with an area per molecule of ca. 29 Å^2).

(34) Oxygen had to be removed from the aqueous solution prior to photopolymerization, since the presence of oxygen inhibited the polymerization, presumably by quenching diacetylene radicals. Day, D.; Ringsdorf, H. *J. Polym. Sci., Polym. Lett. Ed.* **1978**, *16*, 205−210.

(35) Due to heat generated by the AFM, this corresponds to a true sample temperature of ca. 34 °C.

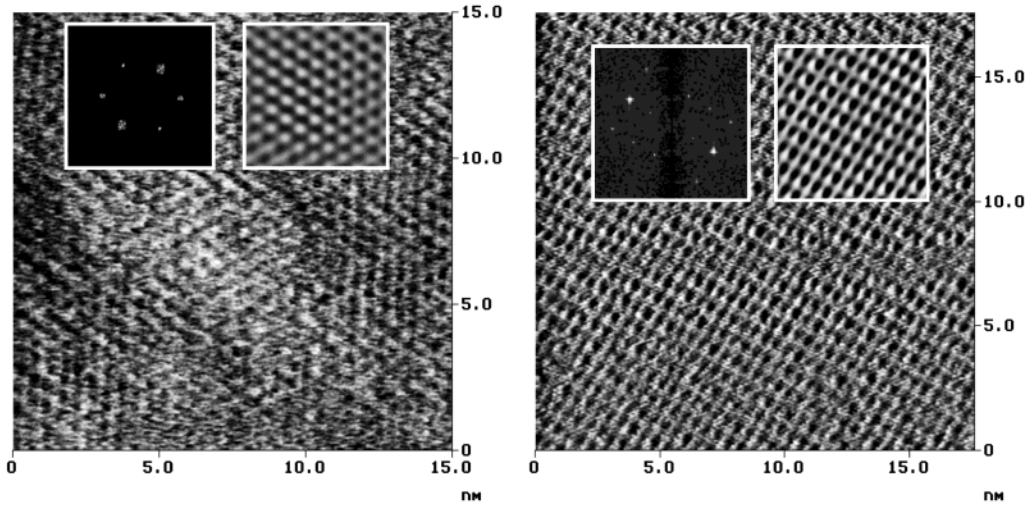

Figure 4. High-resolution CM-AFM images of monolayers of monomeric **1** on glass acquired in air: (a) height image of freshly prepared sample; (b) deflection image of aged, restructured lipid layer. Insets: 2-D FFT, autocovariance filtered sections.

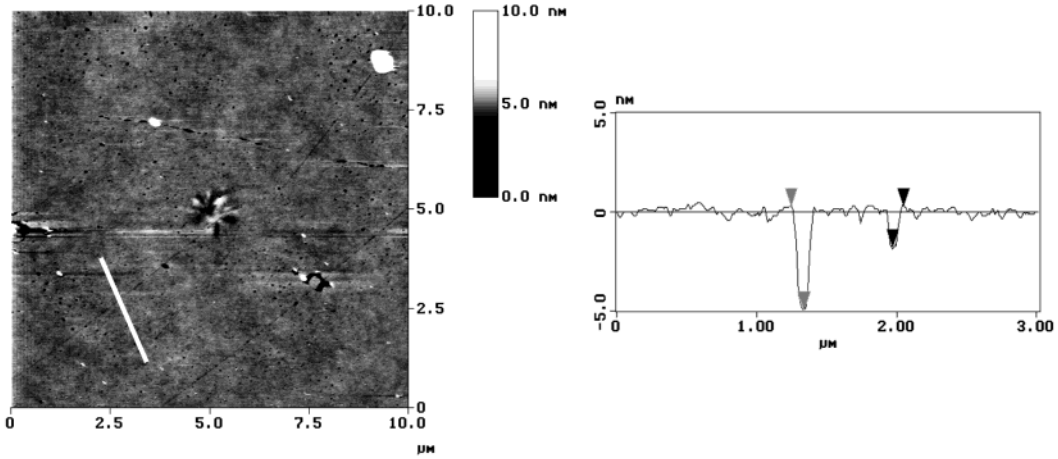

Figure 5. (a) CM-AFM height image of a monomeric bilayer of **1** recorded in water; (b) height profile along the white line of (a). The step heights indicated by the markers are 5.4 and 2.8 nm, respectively.

This increase in area per molecule is consistent with an increase in tilt angle of the molecules with respect to the surface-normal direction.

After transfer of the second layer of **1** using the LS technique, the AFM measurements were carried out in water. Both TM-AFM (no data shown) and CM-AFM revealed a smooth bilayer with scattered defects (Figure 5a). The number of defects is significantly increased compared to the monolayer discussed above. This observation may be related to the difference in transfer procedure (LB versus LS). The rms roughness of the monomeric bilayer was measured to be 0.5 ± 0.23 nm. The section analysis (Figure 5b) shows step heights of ∼3.0 and ∼5.6 nm at defect sites in the bilayer, which agree well with the expected heights of the monolayer and bilayer.

High-resolution CM-AFM images recorded in water unveiled a periodic lattice structure on the nanometer scale (Figure 6). This lattice is clearly different from the structure observed for the monolayer (Figure 4a). From the two-dimensional fast Fourier transform (FFT), we calculate a rectangular lattice (a_2 = 11.3 Å, b_2 = 5.8 Å corresponding to an area requirement of 66 Å^2/molecule), which is consistent with the packing of the lipid headgroups.

The bilayers stayed under water at all times during the experiments and were found to be stable for a period longer than 100 days in water. Exposing these layers to air without rinsing led to a characteristic collapse of the bilayer structure. A typical TM-AFM image recorded in air is shown in Figure 7a. The step height, as measured in cross-sectional plots (Figure 7b), was 5.5 nm. Careful

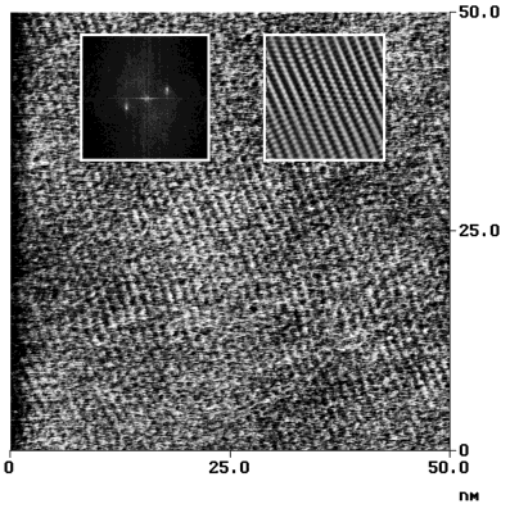

Figure 6. High-resolution CM-AFM friction image of a monomeric bilayer of **1** acquired in water (insets: 2-D FFT, autocovariance filtered section).

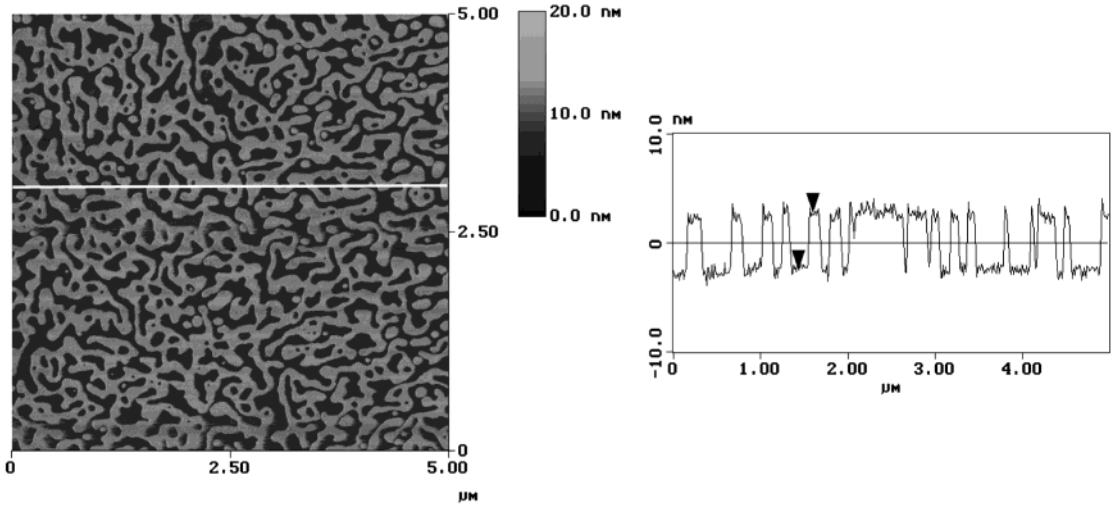

Figure 7. (a) TM-AFM image of collapsed monomeric bilayer of **1** imaged in air; (b) height profile along the white line in (a). The step height indicated by the markers is 5.2 nm.

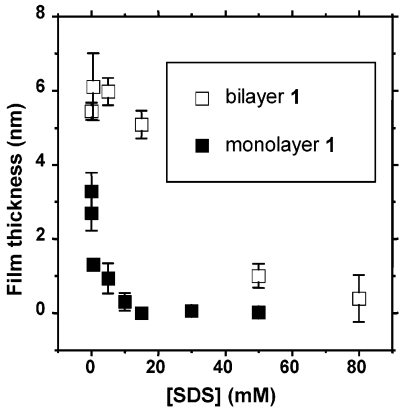

Figure 8. Dissolution of monolayers and bilayers of **1** from oxidized silicon surface by SDS solutions. The films were immersed in SDS solutions of various SDS concentrations for 30 min, and the remaining film was measured by null ellipsometry.

rinsing with water removed the collapsed bilayer film completely (no data shown). Based on these observations, the transfer of *intact* bilayers into the AFM liquid cell could be verified.

Solubilization of Monomeric 1 in Monolayers and Bilayers. One of the components of our micropatterning strategy is to selectively remove monomeric lipids by an organic solvent or by a detergent solution. In the current study, we have employed sodium dodecyl sulfate (SDS) solution as the solubilization agent. Figure 8 shows the solubilization efficiency of monomeric **1** monolayers and bilayers from oxidized silicon surfaces as a function of the concentration of SDS solutions applied. The solubilization was found to be kinetically controlled and depended on various factors, such as efficiency of the solution mixing and immersion time in the SDS solution. However, with constant conditions (30 min immersion without external mixing of the solution) we observed a reproducible removal of **1** from the solid surface. For these controlled conditions, the removal depended only on the SDS concentration.

Higher SDS concentration removed the film more effectively under otherwise constant conditions, as expected. However, monolayers and bilayers of **1** showed markedly different solubilization properties. In the case of monolayers, significant removal of the film occurred even at concentrations below the critical micellar concentration (cmc) of SDS (ca. 0.008 M).[36] In the case of bilayers, the film thickness remained unchanged as long as the SDS concentration was below the cmc. As the SDS concentration was increased beyond the cmc, the thickness of the remaining film gradually decreased. Complete solubilization was achieved if 0.08 M of SDS was used.

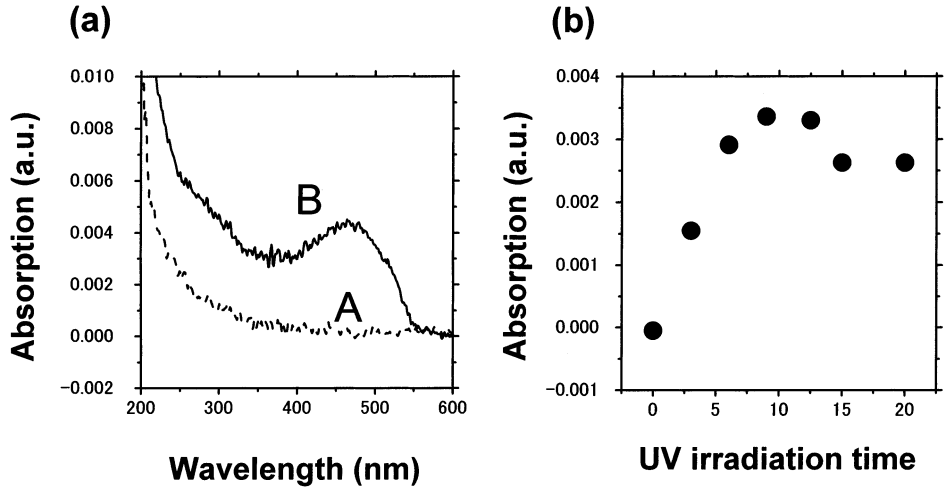

Figure 9. Polymerization of **1** by UV irradiation: (a) UV−visible absorption spectra (A) before and (B) after polymerization for 9 min; (b) dependence of UV absorption intensity at 470 nm on UV light irradiation time.

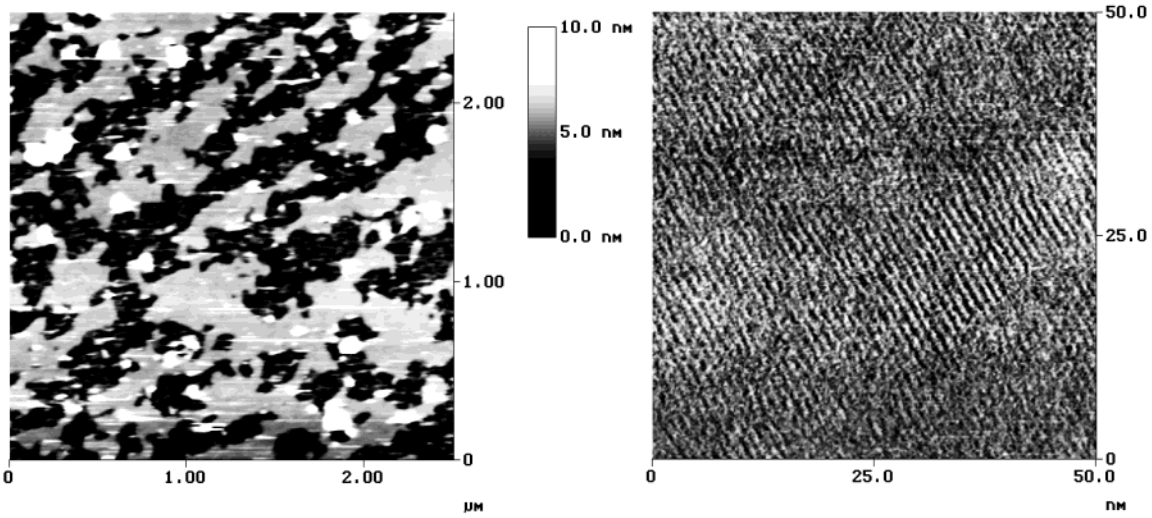

Figure 10. (a) Morphology of homogeneously polymerized bilayers of **1** after SDS treatment as unveiled by CM-AFM in water. (b) The lattice of the phospholipid headgroups was resolved in high-resolution CM-AFM images under water. The duration of UV illumination was 5 min.

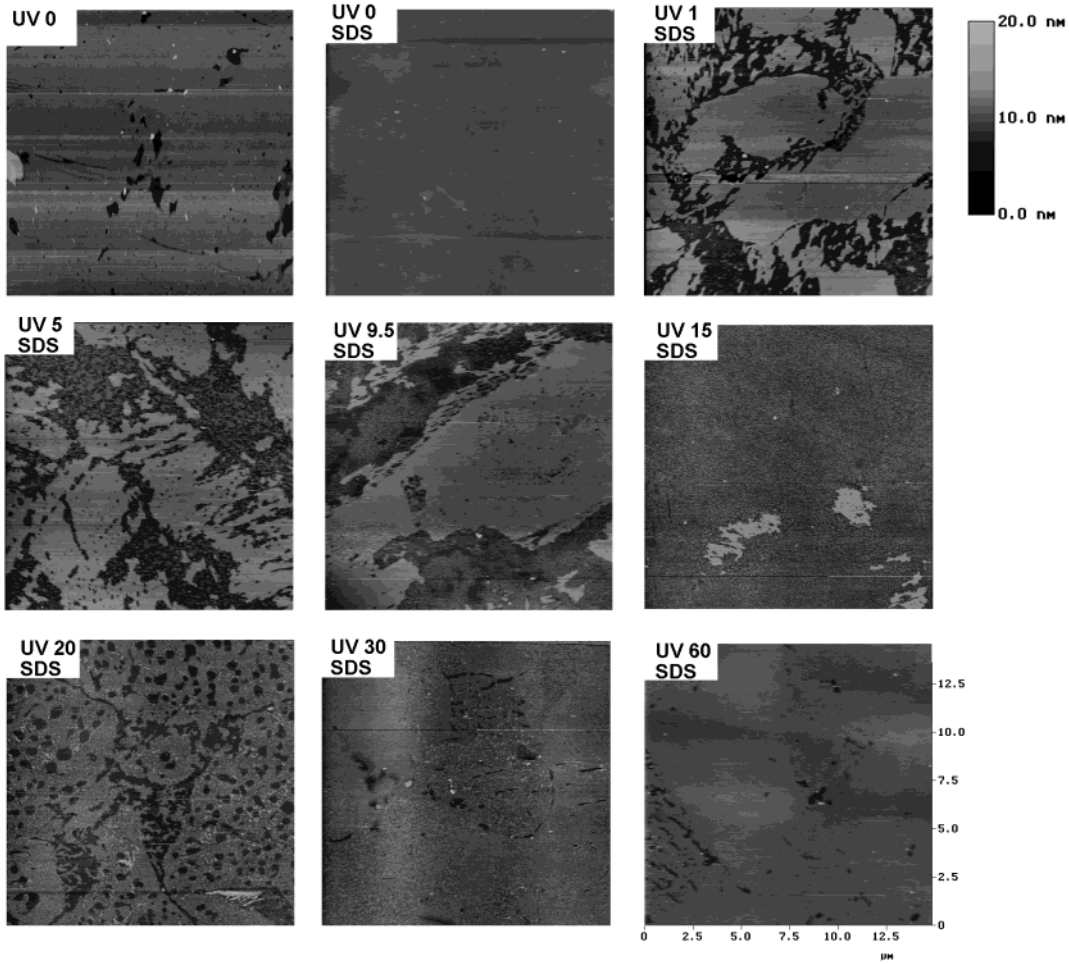

Figure 11. Polymerization of **1** by UV irradiation. The bilayer structures were observed by CM-AFM in water after the photopolymerization and subsequent incubation in 0.08 M SDS solution for 15 h. The UV irradiation time in minutes and the subsequent treatment are indicated.

Since the polymerized bilayers are stable under these conditions (vide infra), we have applied this concentration for the solubilization studies of the partially polymerized bilayers.

Photopolymerization of Bilayers of 1. Polymerization of **1** by UV light (254 nm) results in the formation of conjugated ene−yne backbones. This process could be monitored most conveniently by UV/visible absorption spectroscopy. Figure 9a shows the UV/visible absorption spectra of bilayers of **1** before and after polymerization. The polymeric bilayer has an absorption band between 400 and 550 nm that originates from oligomeric ene−yne backbones. The intensity of this band as a function of the UV irradiation time is plotted in Figure 9b. This graph

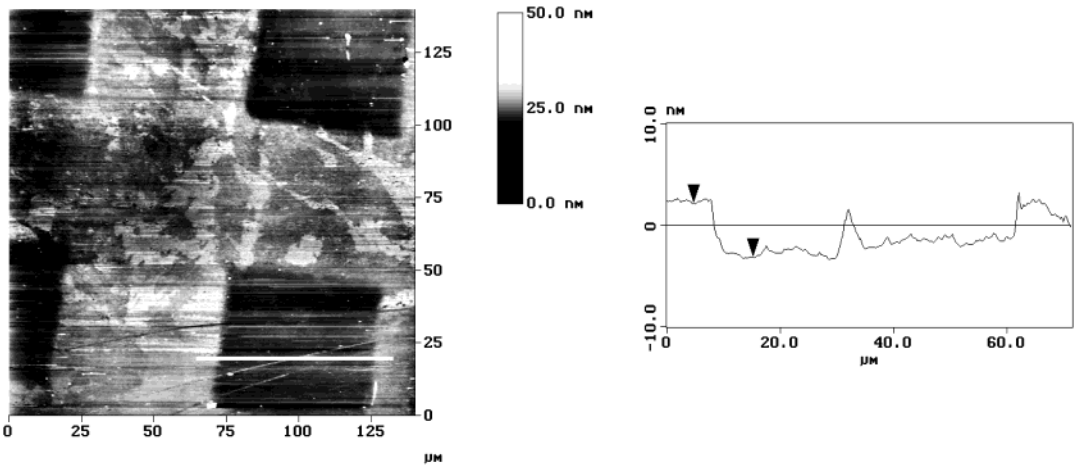

Figure 12. (a) CM-AFM height image of patterned bilayer imaged in water; (b) height profile along the white line in (a). The step height indicated by the markers is 5.9 nm.

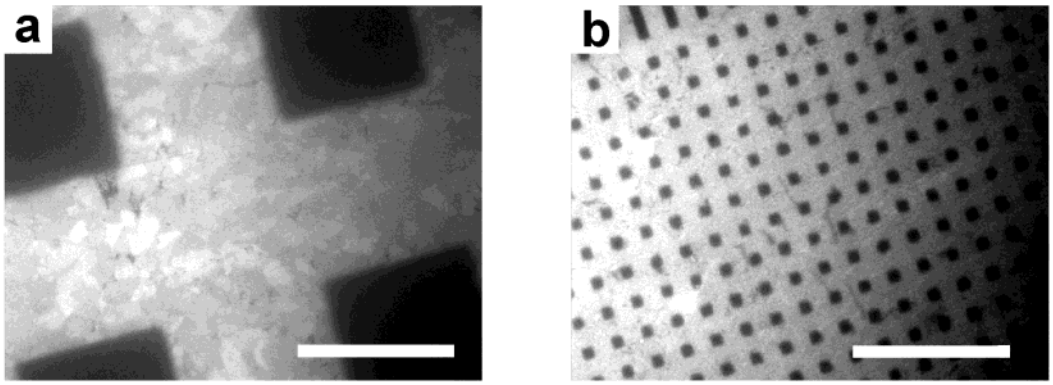

Figure 13. Patterned bilayers: fluorescence microscopy images. The scale bars correspond to 50 μm.

allows us to analyze the relation between the UV light dose and the progress of polymerization. The absorption intensity increased up to 10 min of irradiation and reached a plateau; longer irradiation resulted in a slight decline of the absorption.

The morphological changes in the film during the polymerization process could be studied by AFM. The surface of a homogeneously polymerized bilayer of **1**, which may be observed in the patches seen in Figure 10a, appeared to be as smooth as the unpolymerized bilayers shown in Figure 5. The lattice of the lipid bilayer could be resolved in high-resolution CM-AFM images (Figure 10b), which revealed a lattice structure similar to that of the monomeric bilayers.

The morphological development of the bilayer films as a function of polymerization time was investigated systematically. Figure 11 summarizes the observed film morphologies after various durations of photopolymerization and subsequent treatment with 0.08 M SDS (ca. 15 h). The unpolymerized **1** bilayer was removed completely by the SDS treatment. For the samples with a short UV exposure, we observed the partial coverage of the substrate with bilayer domains that were presumably polymeric. The height difference between the bilayer domains and the glass substrate was ca. 5.5 nm. As we applied a longer UV irradiation time, a larger surface area was covered by the bilayers (see the image for 9.5 min UV irradiation). However, longer UV irradiation seemed to induce the following two effects: (i) increase in the surface roughness; (ii) decrease of the average film thickness.

Micropatterning. Micropatterning of the bilayers was achieved by placing a contact lithography mask on the bilayer surface during the photopolymerization. Figure 12a shows the AFM image of a micropatterned bilayer of **1** that was polymerized for 30 min and treated with a 0.08 M SDS solution. It is evident that the bilayers in the protected areas (squares), which remained monomeric, were removed by the SDS solution. The remaining polymeric bilayer looks heterogeneous with many patches of slightly higher plateaus. In cross-sectional plots (Figure 12b), we measured a height difference between the substrate and the remaining film of ca. 5.9 nm.

Fluorescence microscopy under water also showed a heterogeneous bilayer morphology that resembled the CM-AFM data (Figure 13). The square areas did not show fluorescence at 488 nm, while the surrounding areas showed fluorescence emission with different intensities.

Upon exposure to air, the polymerized bilayer structure collapsed partially, as seen in CM-AFM height images (Figure 14a). However, this morphology is very different compared to the collapsed monomeric bilayers of **1** (Figure 7). The friction force microscopy image shown in Figure 14b reveals homogeneous friction contrast in the different areas of the pattern. A similarly well-defined pattern is observed in tapping mode AFM images (Figure 14c,d).

(36) Since monolayers have a hydrophobic surface facing the aqueous solution, their structure is supposed to be energetically less favorable in water compared with bilayers. However, water alone did not remove monolayers from the surface, as evidenced by the observation that the film thickness remained unchanged, if a monolayer was immersed in water for the same period of time. SDS monomers may adsorb onto the hydrophobic monolayer surface and cause premicellar aggregation that solubilizes **1** molecules.

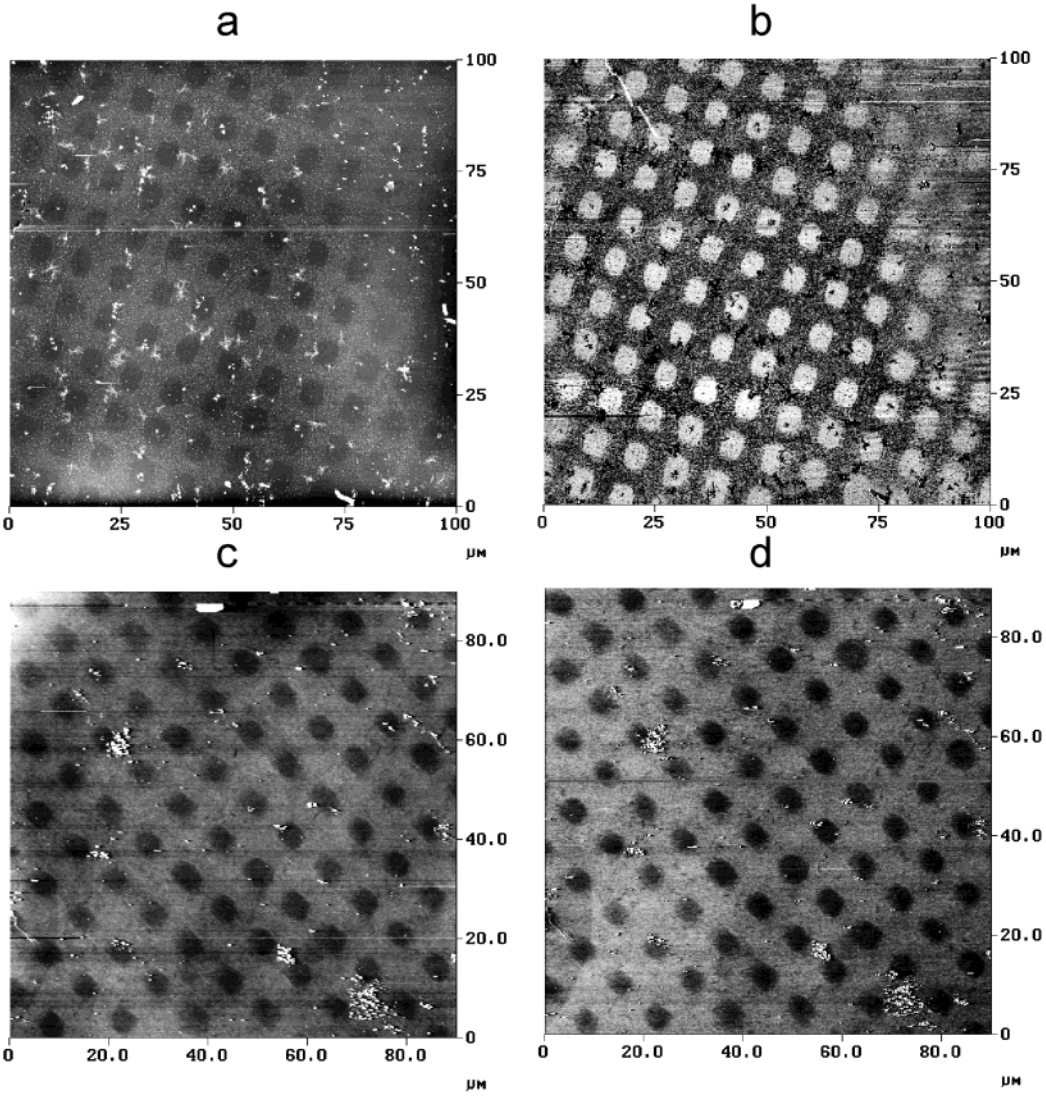

Figure 14. AFM images of a patterned bilayer membrane recorded in air. (a) CM-AFM height (*z*-scale 50 nm) and (b) friction images (friction force increases from dark to bright). (c) TM-AFM height (*z*-scale 20 nm) and (d) phase images (phase angle shift increases from dark to light).

Discussion

In the current study, multimode AFM measurements have been carried out to characterize the first three steps of the micropatterning strategy depicted in Figure 1. The morphology and defect structures were imaged with tapping mode AFM and contact mode AFM, respectively; in some cases, the nanometer-scale arrangement of alkyl tails or lipid headgroups was visualized.

The monomeric Langmuir monolayer of **1** transferred onto glass substrates had a roughness comparable to the bare glass substrate and showed few defects. These defects consisted mainly of dust particles and shallow depressions. The depth of these depressions (measured as step height in cross-sectional plots) of ca. 1.3 nm (Figure 3) does *not* correspond directly to the monolayer height since it is unlikely that the bare substrate is exposed at the defects observed or that the AFM tip can reach to the substrate. This interpretation is corroborated by the observation of larger defects in the bilayer structures prepared subsequently by the LS technique. Here step heights of ca. 3.0 nm and ca. 5.6 nm were measured, which can be attributed to defects in the top leaflet of the bilayer membrane or to defects of the complete lipid bilayer, respectively (Figure 5). The same observation was made when the bilayer structure was intentionally disrupted in CM-AFM at high force. The experimentally determined thicknesses agree well with the calculated values based on the molecular structure (Figure 2), assuming an all-trans conformation of the hydrocarbon tails.

In addition to the thickness measured at defect sites, the molecular-scale order in the monolayers and bilayers was found to be consistent with the anticipated structural organization of the assemblies depicted schematically in Figure 1. The monolayers exposed the alkane tail to the air, as can be concluded from the area requirement per molecule of ca. 29 Å^2 deduced from the high-resolution CM-AFM images (Figure 4a). By contrast, the area requirement of ca. 66 Å^2 agrees well with a tightly packed array of phospholipid headgroups; thus, in the bilayers the lipid headgroups are exposed to the aqueous phase (Figure 6). On the basis of all these experiments, we conclude that the structure of monolayers and bilayers of **1** deposited onto glass substrates by LB and subsequent LS techniques is indeed most consistent with the expected layer structures.

The photopolymerization proceeds without disruption of the bilayer architecture, as can be concluded from the CM-AFM data shown in Figure 10, where we find a lattice

spacing for the photopolymerized phospholipid headgroups that is similar to the monomers. The AFM observations of patterned samples (Figures 12 and 14) also have shown that the polymerized bilayers are resistant to solubilization by SDS solutions. The dissolution with SDS is kinetically controlled (vide supra), and the procedure established here (at concentrations above the solution cmc of SDS) leads to a complete removal of the unpolymerized, i.e., monomeric, bilayer of **1**. The successful removal of the unpolymerized bilayer was independently validated by CM-AFM carried out in SDS solution (no data shown) and is further evident from the AFM data shown in Figures 12 and 14. In the latter images, the collapsed patterned bilayer has been imaged in air, and a very clear contrast between the bilayer regions and the empty squares can be observed. The friction and phase contrast (Figure 14) are related to the difference in mechanical[37−39] and chemical[40,41] properties of the polymerized areas vs the unpolymerized and subsequently dissolved monomeric areas (i.e., glass). The high friction forces and the pronounced phase lag observed in the squares is consistent with the interpretation that bare glass (high surface energy) is exposed, and the low friction forces observed in the surrounding matrix suggest the presence of a low surface energy layer. The observed features of the polymerized domains are in clear contrast to the case of monomeric bilayers that show a characteristic collapsed structure upon exposure to air (Figure 7).

However, the experiments with various UV doses (see, e.g., Figure 11) suggest that the polymerization either does not proceed homogeneously or that UV light-induced degradation of the film competes with the rather slow polymerization (vide infra). Similar to the AFM data (Figure 12), where the height differences are directly measured, bright, i.e., highly fluorescent, patches were observed by fluorescence microscopy (Figure 13). In the UV spectra it was evident that longer irradiation times resulted in a slight decline of the absorption for the band attributed to the conjugated polymeric backbone. These observations might indicate side reactions (degradation or depolymerization) or a reorganization of the bilayer films during the photopolymerization process.[42]

The observation of the solubilization-resistant bilayers after a very short UV irradiation, as shown in Figure 11, does *not* agree with our previous view of the polymerization process. Previously, we have assumed that the polymerization proceeds homogeneously within the whole bilayer and the cross-linking occurs gradually after sufficient UV irradiation.[9] By contrast, the new data indicate that parts of the bilayer become resistant to the solubilization with a small dose of UV light.

The observed local differences in solubility (Figure 11) are likely the result of spatially heterogeneous polymerization behavior. Since the illumination intensity can be assumed to be constant on the relevant sub-λ length scales, we postulate that the observed local differences are caused by heterogeneous polymerization due to differences in local packing; i.e., there is a coexistence of domains with different molecular organization. Such differences in local packing or molecular organization would result in spatially different degrees of polymerization and thus different resistance to solubilization by SDS.

From the above observations, we can draw the following summary. To achieve an effective patterning of bilayer membranes, the basic requirements for the polymerization process are that the polymerization proceeds to a completion to build a fully cross-linked polymeric network, and that the bilayer structures remain intact during the polymerization process. The current AFM observations suggest that the general bilayer structures of **1** are preserved during the polymerization process such that micropatterning of biomimetic membranes based on lithographic photopolymerization is basically feasible. However, at a more microscopic level, AFM also revealed the possible reorganization of the films during the photopolymerization. It is important for the further development of micropatterned membranes to understand how such reorganization affects the properties of polymeric bilayers as a matrix and as a diffusion barrier for fluid biomimetic membranes.

Acknowledgment. H.S. gratefully acknowledges financial support by the Deutsche Akademischer Austauschdienst (DAAD) in the framework of the "Hochschulsonderprogramm III" and the NSF MRSEC Center on Polymer Interfaces and Macromolecular Assemblies (CPIMA) under DMR 9808677.

LA034078F

(37) Carpick, R. W.; Salmeron, M. *Chem. Rev.* **1997**, *97*, 1163−1194.
(38) Schönherr, H.; Vancso, G. J. *Mater. Sci. Eng., C* **1999**, *8*−*9*, 243−249.
(39) Magonov, S. N.; Elings, V.; Whangbo, M.-H. *Surf. Sci.* **1997**, *372*, L385−L391.
(40) Frisbie, C. D.; Rozsnyai, L. F.; Noy, A.; Wrighton, M. S.; Lieber, C. M. *Science (Washington, D.C.)* **1994**, *265*, 2071−2074.
(41) Noy, A.; Sanders, C. H.; Vezenov, D. V.; Wong, S. S.; Lieber, C. M. *Langmuir* **1998**, *14*, 1508−1511.
(42) It should be noted that the wavelength and intensity of the UV adsorption band do not correlate directly to the *real* degree of polymerization, since the effective conjugation length is limited by the local conformation of polymer backbones and the absorption band does not represent longer polymer chains.